


# CCL21-Ser expression in melanoma cells recruits CCR7<sup>+</sup> naïve T cells to tumor tissues and promotes tumor growth

Megumi Miyamoto<sup>1</sup> | Yuki Kawato<sup>2</sup> | Ryonosuke Fujie<sup>1</sup> | Kaoru Kurowarabe<sup>1</sup> |  
Kakeru Fujiwara<sup>1</sup> | Reika Nobusawa<sup>1</sup> | Ryota Hayashi<sup>1</sup> | Kei Iida<sup>1,2</sup> | Izumi Ohigashi<sup>3</sup> |  
Haruko Hayasaka<sup>1,2,4</sup> 

<sup>1</sup>Department of Science, Graduate School of Science and Engineering, Kindai University, Osaka, Japan

<sup>2</sup>Faculty of Science and Engineering, Kindai University, Osaka, Japan

<sup>3</sup>Division of Experimental Immunology, Institute of Advanced Medical Sciences, University of Tokushima, Tokushima, Japan

<sup>4</sup>Research Institute for Science and Technology, Kindai University, Osaka, Japan

## Correspondence

Haruko Hayasaka, Faculty of Science and Engineering, Department of Science, Graduate School of Science and Engineering, Kindai University, 3-4-1, Kowakae, Higashiosaka, Osaka 577-8502, Japan.

Email: [hhayasaka@life.kindai.ac.jp](mailto:hhayasaka@life.kindai.ac.jp)

## Abstract

CCL21-Ser, a chemokine encoded by the *Ccl21a* gene, is constitutively expressed in the thymic epithelial cells and stromal cells of secondary lymphoid organs. It regulates immune cell migration and survival through its receptor CCR7. Herein, using CCL21-Ser-expressing melanoma cells and the *Ccl21a*-deficient mice, we demonstrated the functional role of cancer cell-derived CCL21-Ser in melanoma growth in vivo. The B16-F10 tumor growth was significantly decreased in *Ccl21a*-deficient mice compared with that in wild-type mice, indicating that host-derived CCL21-Ser contributes to melanoma proliferation in vivo. In *Ccl21a*-deficient mice, tumor growth of melanoma cells expressing CCL21-Ser was significantly enhanced, suggesting that CCL21-Ser from melanoma cells promotes tumor growth in the absence of host-derived CCL21-Ser. The increase in tumor growth was associated with an increase in the CCR7<sup>+</sup> CD62L<sup>+</sup> T cell frequency in the tumor tissue but was inversely correlated with Treg frequency, suggesting that naïve T cells primarily promote tumor growth. Adoptive transfer experiments demonstrated that naïve T cells are preferentially recruited from the blood into tumors with melanoma cell-derived CCL21-Ser expression. These results suggest that CCL21-Ser from melanoma cells promotes the infiltration of CCR7<sup>+</sup> naïve T cells into the tumor tissues and creates a tumor microenvironment favorable for melanoma growth.

## KEYWORDS

CCL21, CCR7, chemokine, melanoma, naïve T cell

**Abbreviations:** DCs, dendritic cells; KO, knockout; LN, lymph node; MDSCs, Myeloid-derived suppressor cells; TDLNs, tumor-draining LNs; TLS, tertiary lymphoid structures; Tregs, regulatory T cells; WT, wild-type.

This is an open access article under the terms of the [Creative Commons Attribution-NonCommercial](https://creativecommons.org/licenses/by-nc/4.0/) License, which permits use, distribution and reproduction in any medium, provided the original work is properly cited and is not used for commercial purposes.

© 2023 The Authors. *Cancer Science* published by John Wiley & Sons Australia, Ltd on behalf of Japanese Cancer Association.

## 1 | INTRODUCTION

Chemokines are classified into inflammatory and homeostatic chemokines. Inflammatory chemokines are induced to be expressed in tissues by inflammatory stimuli and promote the migration of effector lymphocytes into the tissues, whereas homeostatic chemokines are chemokines expressed in specific tissues in noninflammatory conditions. The homeostatic chemokine CCL21-Ser is encoded by the *Ccl21a* gene and is expressed in the stromal cells of secondary lymphoid tissues and thymic epithelia.<sup>1-4</sup> CCL21-Ser selectively binds to the chemokine receptor CCR7, which is expressed on the plasma membrane of various immune cells, including thymocytes, naïve lymphocytes, central memory T cells, regulatory T cells (Tregs), and mature dendritic cells (DCs).<sup>5,6</sup> The critical roles of the CCL21/CCR7 axis in the acquired immune system have been demonstrated by gene knockout (KO) studies in mice. The *Ccr7*-KO mice showed a reduction in primary acquired immune response due to an impaired T cell and DC migration into the secondary lymphoid tissues.<sup>7</sup> The *plt/plt* mice, the mutant mice deficient in CCR7 ligands, CCL19 and CCL21-Ser, showed decreased numbers and abnormal localization of T cells in secondary lymphoid tissues and prolonged immune responses.<sup>8</sup> The *Ccr7*-KO and *plt/plt* mice were defective in the cortex-to-medulla migration of thymocytes, resulting in a disturbed central tolerance.<sup>9</sup> The *Ccl21a*-KO mice showed autoimmune disease-like symptoms, including incomplete removal of autoreactive T cells in the thymus and lymphocytic infiltration of the lacrimal and salivary glands.<sup>3</sup> The study of *Ccl21a*-KO mice demonstrated that CCL21-Ser presentation at the vascular region contributes to mature T cell emigration from the neonatal thymus to the peripheral tissues, suggesting that CCL21-Ser plays an essential role in the formation of T cell pools in the thymus and peripheral tissues.<sup>10</sup>

Clinically, CCR7 is expressed in malignant tumor cells, such as breast cancer, malignant melanoma, gastric cancer, non-small cell lung cancer, esophageal squamous cell carcinoma, and chronic lymphocytic leukemia, and the CCR7 expression levels have been reported to positively correlate with lymph node (LN) metastasis.<sup>11-13</sup> Melanoma cells experimentally expressing high levels of CCR7 acquire the ability to metastasize to the LNs.<sup>14</sup> Breast cancer cells with an increased CCR7 expression metastasize to the lungs showed an increased LN metastatic potential,<sup>15</sup> suggesting that CCR7 signaling is involved in cancer metastatic cancer tropism. In B16-derived melanoma, CCL21-Ser secreted by melanoma cells themselves or by nontumor cells regulate tumor growth.<sup>16,17</sup> A previous report demonstrated that melanoma cells with high CCL21-Ser expression resulted in enhanced tumor growth in vivo, whereas melanoma cells with reduced CCL21-Ser expression diminished tumor growth.<sup>16</sup> However, not only melanoma cell-derived CCL21-Ser but also host cell-derived CCL21-Ser, such as tumor-associated fibroblasts and blood vessels responsible for immune cell migration into melanoma tissue, may indirectly support tumor growth. In a previous study, CCL21-Ser expression in melanoma cells induced LN-like structures in the tumors and increased the recruitment of Tregs and bone marrow-derived immunosuppressive cells to the tumors.<sup>16</sup> In

contrast, Peske et al. (2015) demonstrated that B16-derived tumors develop LN-like vasculature expressing CCL21-Ser, recruiting naïve lymphocytes into the tumor tissue to enhance antitumor immunity.<sup>17</sup> Therefore, it is controversial whether CCL21-Ser expression promotes or inhibits melanoma growth, and the exact contribution of melanoma cell-derived CCL21-Ser to the tumor microenvironment has been poorly studied.

We have previously demonstrated that melanoma growth is significantly decreased in *Ccl21a*-KO mice, suggesting that the host-derived CCL21-Ser promotes immune cell infiltration into the tumor tissues and supports tumor growth.<sup>18</sup> In this study, we explored the contribution of CCL21-Ser derived from melanoma cells using *Ccl21a*-deficient mice, where the possibility of host-derived CCL21-Ser's effects is completely ruled out.

## 2 | MATERIALS AND METHODS

### 2.1 | Cells

The mouse melanoma cell line B16-F10 was obtained from the American Type Culture Collection. Cells were cultured in DMEM (FUJIFILM Wako Pure Chemicals) supplemented with 10% (v/v) fetal calf serum, 2 mM L-glutamine, 1 mM sodium pyruvate, 100 U/mL penicillin, 100 µg/mL streptomycin, 50 µM 2-mercaptoethanol, 0.1 mM nonessential amino acids, and 10 mM HEPES (Nacalai Tesque). The cells expressing mouse CCL21-Ser were established as follows. Total RNA was extracted from a C57BL/6 LNs using FastGene RNA Premium Kit (NIPPON Genetics). After conversion to cDNA using Fast gene Scriptase II cDNA 5x Ready Mix (NIPPON Genetics), the DNA fragment corresponding to the mouse *Ccl21a* full-length cDNA was treated with restriction enzymes XhoI (TaKaRa) and NotI (New England Biolabs Japan) and was inserted into the pCAGI-puro vector (kindly provided by Dr. J. Miyazaki, Osaka University). The plasmid harboring *Ccl21a* and the pCAGI-puro vector was transfected into B16-F10 cells by the PEI-MAX (Polysciences) according to the manufacturer's instructions and cultured in a culture medium containing 1 µg/mL puromycin to establish drug-resistant cells.

### 2.2 | Animals

The experimental protocols for the use of laboratory animals were approved by the Ethics Review Committee of Kindai University (KASE-2021-001). C57BL/6, *Ccl21a*-KO, and B6 Albino (B6N-*Tyr<sup>c-Brd</sup>/BrdCrCrI*) mice with *Ccl21a*-KO background were obtained as previously described.<sup>18</sup> GFP transgenic mice, C57BL/6-Tg(CAG-EGFP), were purchased from Nihon SLC (Hamamatsu, Japan). For in vivo tumor formation, cells ( $1 \times 10^6$  cells) were subcutaneously injected into the right ventral region of the six-week-old mice of either sex. Two weeks later, the mice were killed by isoflurane anesthesia, and the tumor weights were measured. Statistical analysis was performed using the Steel-Dwass test.

## 2.3 | RT-PCR analysis and measurement of CCL21-Ser concentration by ELISA

RT-PCR was performed as previously described.<sup>18</sup> The cell culture supernatant was diluted 100-fold with PBST (0.1% PBS containing 0.05% Tween20), added dropwise to a 96-well microplate, and immobilized for 2 h. The wells were treated with 200 ng/mL biotinylated anti-mouse CCL21 antibody (BAF457, R&D Systems) for 1 h. After washing five times with PBST, the wells were treated with HRP-conjugated streptavidin (1:5000 dilution with PBST containing 0.1% BSA, Perkin Elmer) for 1 h. Absorbance at 650 nm was measured using a MultiScan spectrophotometer (Thermo Fisher Scientific) 15 min after the addition of SureBlue tetramethylbenzidine (TMB) peroxidase Substrate (SeraCare Life Sciences).

## 2.4 | In vitro cell proliferation assay

Cells were seeded into three wells of a 24-well plate at  $1 \times 10^3$  cells per well. On Days 1, 3, and 5, cells were treated with PBS containing 0.25% Trypsin and 1 mM EDTA, and the number of cells in each well was counted with a hemocytometer.

## 2.5 | In vivo bioluminescence imaging

Cells ( $1 \times 10^6$  cells) stably transfected with pCR3.1-Uni plasmid (Invitrogen) harboring the click beetle luciferase gene were injected subcutaneously into the backs of 4–6 week-old wild-type or *Ccl21a*-KO mice with B6 Albino backgrounds. The mice were imaged using an IVIS Imaging System (Caliper Life Sciences) after intraperitoneal injection with 3 mg (150 mg/kg) D-luciferin (VivoGlo; Promega).

## 2.6 | Adoptive transfer

Splenocytes ( $5 \times 10^6$  cells) from the GFP transgenic mice were injected into the tail vein of the recipient melanoma-bearing mice. Single-cell suspensions from tumor tissues, spleen, and inguinal LNs were prepared from the mice 24-h after cell injection.

## 2.7 | Flow cytometry

The tumor tissues were shredded to approximately 1–2 mm in RPMI-1640 medium containing 0.1% BSA on ice, enzymatically treated at 37°C for 1.5 h with RPMI 1640 medium containing 0.1% BSA, 1 mg/mL collagenase type I (9001-12-1; Wako), and 2 µg/mL deoxyribonuclease I (9003-98-9; Sigma), and were subsequently treated with 0.83% NH<sub>4</sub>Cl and 0.17 M Tris-Cl (pH 7.65) for erythrocyte hemolysis. LN cells were isolated by gently scraping LNs with glass slides on ice in RPMI-1640 medium containing 0.1% BSA. The cells were passed through a nylon filter (pore size 108 µm) to obtain single-cell suspensions and treated with HB-197 cell culture supernatant containing an anti-CD16/32

(Fc-γ receptor) antibody. After washing with FACS buffer (PBS containing 0.1% BSA, 100 U/mL penicillin, 100 µg/mL streptomycin), cells were treated with antibodies for 30 min on ice. To detect IFN-γ expression, the tumors were treated with the tissue digestion medium containing a protein transport inhibitor (BD GolgiStop Protein Transport Inhibitor, BDB545724; BD Biosciences). After staining with antibodies against cell surface molecules, cells were washed twice with 1×BD Perm/Wash Buffer and treated with Fixation and Permeabilization Solution (554,722; BD Biosciences) for 20 min on ice, and then treated with anti-IFN-γ antibody or rat IgG isotype control for 1 h on ice. For FoxP3 detection, after staining with antibodies against cell surface molecules, the cells were washed twice with True Nuclear 1× Perm Buffer and then treated with True Nuclear 1× Fix Concentrate (424,401, BioLegend) for 1 hour at room temperature. After washing twice with True Nuclear 1×Perm Buffer, cells were subjected to staining with anti-mouse FoxP3 antibody or rat IgG isotype control for 1 hour at room temperature. The information and concentrations of the antibodies used in this study are shown in Table 1. The cell number was counted with Flow-Count Fluorospheres (Beckman Coulter). The data analysis and interpretation were performed on a BD LSRFortessa system and the FlowJo software (Nippon BD).

## 2.8 | Profiling of immune cell components in human melanoma samples

The abundance of immune cell components was analyzed by the CIBERSORTx program using the standard LM22 signature matrix<sup>19,20</sup> based on the transcriptome profiles of 442 cases described as “Malignant melanoma, NOS” extracted from The Cancer Genome Atlas (TCGA) (<https://www.cancer.gov/ccg/research/genome-sequencing/tcga>). To improve the accuracy of profiling, 56 melanoma signature genes were applied to the CIBERSORTx algorithm, and the cell types processed in the original LM22 dataset were recalculated. The total estimated cell fraction was set to 1.0. Finally, 387 samples with an estimated rate of melanoma fraction ranging from 0.20 to 0.95 were analyzed.

## 2.9 | Statistics

The data were analyzed by the Mann–Whitney *U*-test, the Kruskal–Wallis test with the Steel–Dwass post hoc test using the “R” statistical software, Student's *t*-test, or one-way ANOVA with Tukey's test using StatPlus software version v7 (AnalystSoft).

# 3 | RESULTS

## 3.1 | Contribution of host- and melanoma cell-derived CCL21-Ser to tumor growth

To investigate the contribution of melanoma cell-derived CCL21-Ser to tumor growth, we established the F10-ccl21 cells, a stable cell line transfected with a plasmid encoding mouse CCL21-Ser in B16-F10

TABLE 1 List of reagents and resources used for flow cytometry.

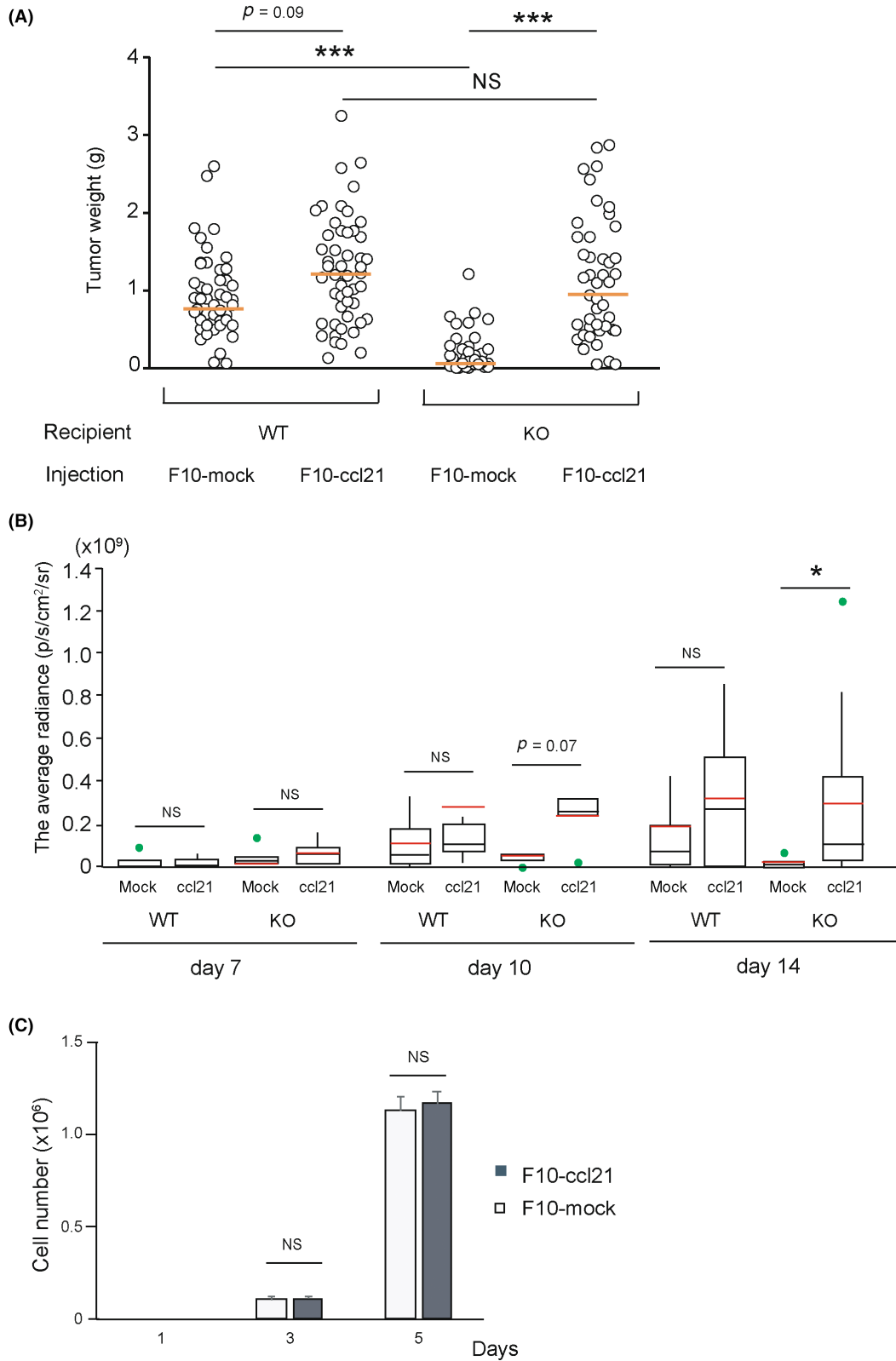
Reagent or Resource	Source	Clone	Concentration ( $\mu\text{g}/\text{mL}$ )	RRID
FITC anti-mouse CD3 $\epsilon$	BioLegend	145-2C11	5	AB_312671
APC anti-mouse CD8 $\alpha$	BioLegend	53-6.7	2	AB_312751
PE/Cy7 anti-mouse CD45	BioLegend	30-F11	1	AB_312979
FITC anti-mouse CD45	BioLegend	30-F11	1	AB_312973
FITC anti-mouse CD4	BioLegend	RM4-5	2	AB_312713
PE anti-mouse CD4	BioLegend	GK1.5	1.25	AB_312693
Alexa Fluor 647 anti-mouse CD4	BioLegend	GK1.5	2	AB_493519
PE anti-human/mouse CD44	BioLegend	IM7	1	AB_312959
FITC anti-mouse CD62L	BioLegend	MEL-14	2	AB_313093
PE anti-mouse CD25	BioLegend	3C7	2.5	AB_312847
Biotin anti-mouse CD197	BioLegend	4B12	2.5	AB_389231
PE anti-mouse CD197	BioLegend	4B12	2	AB_389357
PerCP/Cy5.5 anti-mouse CD8	BioLegend	53-6.7	1	AB_2075239
Alexa Fluor 647 anti-mouse CD69	BioLegend	H1.2F3	2	AB_492848
APC anti-mouse IFN- $\gamma$	BioLegend	XMG1.2	2	AB_315404
Biotin anti-mouse CD127	Thermo Fisher Scientific	A7R34	2	AB_466589
PerCP/Cy5.5 anti-mouse CD127	BioLegend	A7R34	2	AB_1937273
Alexa Fluor 488 anti-mouse FoxP3	BioLegend	MF-14	2	AB_1089114
APC anti-mouse F4/80	BioLegend	BM8	2	AB_893481
FITC anti-mouse MHC class II	BioLegend	M5/114.15.2	1	AB_313321
Biotin anti-mouse CD11c	eBioscience	N418	2.5	AB_466363
Biotin anti-mouse/human CD11b	BioLegend	M1/70	2	AB_312787
PE anti-mouse Gr-1	eBioscience	6B6-8C5	1	AB_466046
anti-mouse CD45RA	BD Biosciences Pharmingen	14.8	2	AB_394822
DyLight 649	Vector Lab	N/A	1	N/A
PE-conjugated Streptavidin	BioLegend	N/A	1	N/A
7-AAD	BioLegend	N/A	0.5	N/A

cells, and F10-mock, a control cell line with an empty plasmid. We confirmed via RT-PCR analysis that *Ccl21a* was not expressed in the parental B16-F10 or F10-mock cells but in the F10-ccl21 cells (Figure S1a). ELISA further confirmed CCL21-Ser expression by F10-ccl21 cells. The culture supernatant of F10-ccl21 cells caused color evolution of TMB oxidation, whereas no such change was observed in the mock cells (Figure S1b, upper panel). The estimated CCL21-Ser concentration of F10-ccl21 culture supernatant was approximately

600ng/mL after calibration with the recombinant CCL21-Ser (Figure S1b, lower panel).

Our previous studies with *Ccl21a*-KO mice demonstrated that the host-derived CCL21-Ser expression affects B16-F10 growth in vivo.<sup>18</sup> Consistent with our previous results, the growth of the F10-mock-derived tumor was significantly reduced by approximately one-fifth in the *Ccl21a*-KO mice compared with that in wild-type (WT) mice on Day 14 (Figure 1A). In WT mice, the

**FIGURE 1** The host- and melanoma cell-derived CCL21-Ser expression contributes to tumor growth in WT control and the *Ccl21a*-KO mice. (A) Tumors were weighed 2 weeks after injection with cells derived from F10-mock (WT;  $n=47$ , KO;  $n=41$ ) and F10-ccl21 (WT;  $n=54$ , KO;  $n=45$ ). Each plot shows an individual tumor. The data were analyzed by the Steel–Dwass test. Orange lines show the median. \* $p < 0.05$ , NS, not significant. (B) F10-mock and F10-ccl21 cells stably expressing click beetle luciferase were established and subcutaneously injected into WT or *Ccl21a*-KO on the B6 Albino background. Bioluminescence on Days 7, 10, and 14 of wild-type mice with F10-mock ( $n=10$ , 6, 10) and F10-*Ccl21* ( $n=11$ , 7, 11) and KO mice with F10-mock ( $n=9$ , 6, 9) and F10-*Ccl21* ( $n=12$ , 5, 12) were measured. The average radiance of bioluminescence counts measured by IVIS Lumina system ( $\text{p/s}/\text{cm}^2/\text{sr}$ ) is shown. Orange lines show the median. Green dots show mild outliers. The data were analyzed by the Mann–Whitney *U*-test. \* $p < .05$ . (C) In vitro proliferation of B16-F10-derived cell lines stably transfected with the *CCL21a* expression or control plasmid. The cells were seeded in three wells at  $1 \times 10^3$  cells/well, and the number of cells was counted on the indicated days. The graph shows the average values from three independent experiments. The significance test was performed by Student's *t*-test. Error bars indicate SEM. KO, knockout; WT, wild-type.



difference was not statistically significant between F10-ccl21 and F10-mock, although there was an increasing trend with F10-ccl21 injection. In contrast, tumor growth in *Ccl21a*-KO mice increased approximately sixfold after F10-ccl21 injection compared to after F10-mock injection. In vivo bioluminescence imaging showed

a trend toward increased tumor growth in F10-ccl21 over F10-mock on Day 10 and significantly increased on Day 14, supporting the above results (Figure 1B). We also confirmed that there was no significant difference in the in vitro proliferation between F10-ccl21 and F10-mock cells (Figure 1C). These results suggest

that host- and melanoma cell-derived CCL21-Ser support tumor growth *in vivo*.

### 3.2 | CCL21-Ser expression affects the frequency of tumor-infiltrating T cells

The rejection of the highly tumorigenic, poorly immunogenic B16 melanoma is dependent on effector CD8 T cell infiltration.<sup>21</sup> Our previous studies have demonstrated that a decreased B16-F10 proliferation in *Ccl21a*-KO mice is correlated with increased intratumor infiltration of effector CD8 T cells.<sup>18</sup> To clarify the effect of CCL21-Ser expression on immune cell infiltration into tumor tissues, we performed flow cytometry for immunophenotyping with the gating strategy shown in Figure S2. The number of intratumoral CD3<sup>+</sup> T cells of F10-mock tumor normalized to tumor weight showed an increasing trend in *Ccl21a*-KO over WT mice, whereas the CD3<sup>+</sup> T cell count of F10-ccl21 showed a decreasing trend over F10-mock in *Ccl21a*-KO (Figure 2A). The number of CD4, CD8, naïve (CD44<sup>low</sup> CD62L<sup>+</sup>), and activated T cell subsets in tumor tissues of each cell type showed similar patterns as that of CD3 (Figure 2B,C). Notably, naïve CD4 T cell count was statistically increased in F10-ccl21 tumors compared to F10-mock tumors in WT mice, and a similar trend was observed in KO mice, suggesting that melanoma cell-derived CCL21-Ser supports naïve CD4 T cell infiltration into the tumor. Previous reports have demonstrated that eliminating Tregs evokes effective tumor immunity, leading to tumor regression.<sup>22,23</sup> Therefore, we investigated the possibility that Treg infiltration into the tumor is affected by CCL21-Ser-expression, leading to immunological unresponsiveness of CD8<sup>+</sup> cytotoxic T cells against tumors and enhancing tumor growth. The CD4<sup>+</sup> CD25<sup>+</sup> CD127<sup>low</sup> cell subset, which expresses approximately 90% FoxP3 (Figure S3), was defined as Treg in this study. The Treg count in of the F10-mock tumor was increased in *Ccl21a*-KO compared with WT, whereas it was decreased in F10-ccl21 tumors over the F10-mock tumors in KO mice (Figure 2D). Myeloid-derived suppressor cells (MDSCs) are immunosuppressive regulators that play an important role in tumor progression.<sup>24</sup> The Gr-1<sup>+</sup>CD11b<sup>+</sup> MDSC count normalized to tumor weight was significantly increased in F10-ccl21 tumors in *Ccl21a*-KO mice (Figure 2E). These results suggest that the MDSC count, rather than the Treg count, is positively correlated with melanoma growth driven by melanoma cell-derived CCL21-Ser. We analyzed the tumor-infiltrated F4/80<sup>+</sup> macrophages and DCs (F4/80<sup>-</sup> MHC class II<sup>+</sup> CD11c<sup>+</sup>), which are considered critical regulators of tumor immunity, by presenting tumor antigens to T cells and producing cytokines within tumors.<sup>25,26</sup> Although the macrophage and DC counts in F10-ccl21-derived tumors showed a decreasing trend compared with F10-mock-derived tumors in *Ccl21a*-KO and WT mice, they were not statistically significant (Figure 2F,G). These results suggest that host-derived and melanoma cell-derived CCL21-Ser does not significantly affect macrophage and DC cell counts in tumor tissue.

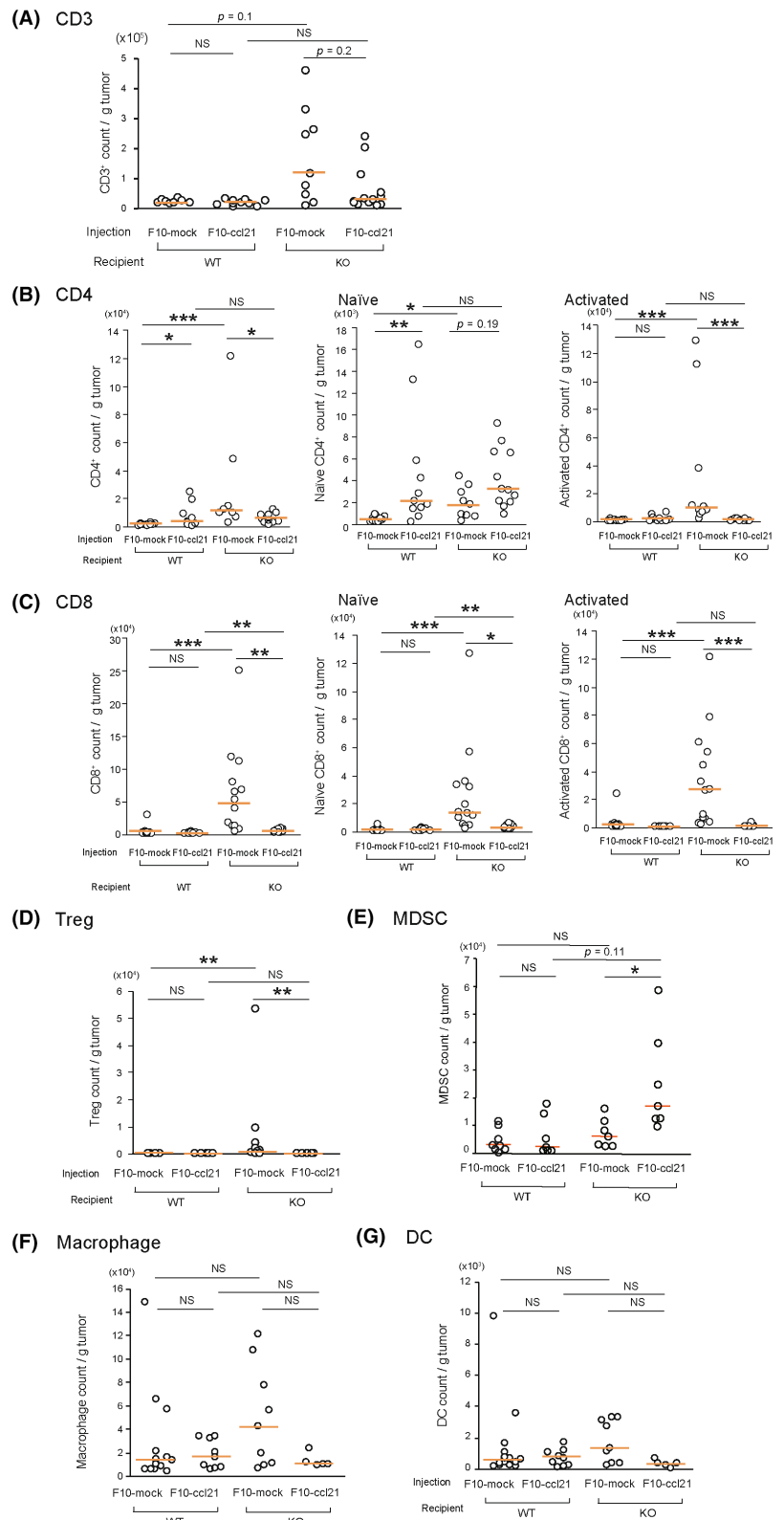
We next examined the frequencies of each immune cell type of intratumoral CD45<sup>+</sup> hematopoietic cells. The CD3<sup>+</sup> T cell percentage of CD45<sup>+</sup> cells was significantly increased in F10-ccl21 tumors compared with the F10-mock tumors in *Ccl21a*-KO and WT mice (Figure 3A). In *Ccl21a*-KO and WT mice, the CD8/CD4 ratio was decreased by melanoma cell-derived CCL21-Ser expression, which is consistent with the results of Figure 2B,C, in which CD4<sup>+</sup> counts in F10-ccl21 tumors were increased in WT mice and CD8<sup>+</sup> counts in F10-ccl21 tumors were more dramatically reduced than CD4<sup>+</sup> counts in *Ccl21a*-KO mice. In CD4<sup>+</sup> and CD8<sup>+</sup> cells, naïve T cell percentages were increased in F10-ccl21 tumors compared with F10-mock tumors (Figure 3B,C). This observation was accompanied by a decrease in the percentage of activated T cells. The percentage of CD4<sup>+</sup> naïve T cells was decreased in F10-mock tumors in *Ccl21a*-KO mice compared with that in WT mice, and it was remarkably restored by the expression of melanoma cell-derived CCL21-Ser (Figure 3B), suggesting that host- and melanoma cell-derived CCL21-Ser contribute to naïve CD4 T cell infiltration into the tumor tissues. In contrast to CD4<sup>+</sup> cells, the percentage of CD8<sup>+</sup> naïve T cells was rather increased in *Ccl21a*-KO mice (Figure 3C), suggesting that the host-derived CCL21-Ser regulates CD8<sup>+</sup> naïve T cell infiltration in a different manner. The frequencies of activated CD8<sup>+</sup> T cells and IFN- $\gamma$  expressing CD8 T cells were inversely correlated with tumor growth, suggesting that effector cells are responsible for the regression of tumor growth (Figure 3C). The frequency of Treg of CD4<sup>+</sup> T cells was significantly reduced in F10-ccl21-derived tumors compared with F10-mock-derived tumors in the *Ccl21a*-KO mice (Figure 3D), suggesting that the melanoma cell-derived CCL21-Ser inhibits Treg infiltration into tumors. Over 95% of the Treg subset identified by FoxP3<sup>+</sup> was CD45RA<sup>-</sup> effector and memory phenotype (Figure S3a), and most of them are CCR7<sup>+</sup> (Figure S3b), suggesting that intratumoral Tregs are mainly central memory phenotype. These results are consistent with the results of previous studies showing that intratumor Tregs are primarily effector and central memory phenotypes.<sup>27</sup> With an increase in naïve T cells between F10-ccl21-derived and F10-mock-derived tumors, MDSCs, macrophage, and DC frequencies relative to CD45<sup>+</sup> hematopoietic cells showed a decreasing trend, although the difference was not statistically significant (Figure 3E-G). These results suggest that host-derived and melanoma cell-derived CCL21-Ser significantly affect T cell composition but do not dramatically affect the composition of MDSCs, macrophages, and DCs in the tumor microenvironment.

### 3.3 | CCL21-Ser expression promotes CCR7<sup>+</sup> CD62L<sup>+</sup> T cell migration in tumors

A series of studies have demonstrated that CCL21-Ser induces immune cell migration via CCR7-mediated signaling.<sup>28</sup> To this end, we assessed the possibility that CCL21-Ser expression promotes CCR7<sup>+</sup> cell recruitment into tumor tissues. The CCR7<sup>+</sup> cell count per tumor weight in F10-mock- and F10-ccl21-derived tumors was comparable

**FIGURE 2** T lymphocyte infiltration is increased in tumors of *Ccl21a*-KO mice.

Tumors derived from F10-mock (WT;  $n=8$ , KO;  $n=9$ ) and F10-ccl21 (WT;  $n=12$ , KO;  $n=13$ ) were dissected 2 weeks after cell injection, and intratumoral immune cell subsets were analyzed by flow cytometry. The intratumoral CD3<sup>+</sup> cell subset was distinguished by the CD45 expression, side scatter profiles, and CD3 expression, and the CD3<sup>+</sup> T count per tumor weight is shown (A). The intratumoral CD4<sup>+</sup> (B) and CD8<sup>+</sup> (C) subset was distinguished by the FSC/SSC profile of tumor cells and CD4 and CD8 expression. (D) Tumor-infiltrated CD4<sup>+</sup> CD25<sup>+</sup> CD127<sup>lo</sup> Tregs in B16-F10-derived tumors in WT and *Ccl21a*-KO mice were analyzed. The plot represents individual tumor samples obtained from three or four experimental repeats with two to four mice in each group. Tumor cells derived from F10-mock tumor (WT;  $n=10$ , KO;  $n=10$ ) and F10-ccl21 tumor (WT;  $n=11$ , KO;  $n=9$ ) were analyzed. The count of (E) myeloid-derived suppressor cells (MDSCs) (Gr-1<sup>+</sup>CD11b<sup>+</sup>), (F) macrophage (F4/80<sup>+</sup>), and (G) dendritic cells (DCs) (F4/80<sup>-</sup> MHC class II<sup>+</sup> CD11c<sup>+</sup>) in an individual tumor sample in WT and *Ccl21a*-KO mice. Tumor cells derived from F10-mock tumor (WT;  $n=10$ , KO;  $n=10$ ) and F10-ccl21 tumor (WT;  $n=9$ , KO;  $n=6$ ) were analyzed. The plot represents individual tumor samples obtained from three or four experimental repeats with two to four mice in each group. The data were analyzed using the Kruskal-Wallis test with the Steel-Dwass post-hoc test. Orange lines show the median. \* $p < 0.05$ , \*\* $p < 0.01$ , NS, not significant. KO, knockout; WT, wild-type.



between *Ccl21a*-KO and WT mice (Figure 4A). However, the proportion of CD45<sup>+</sup> hematopoietic cells of *Ccl21a*-KO tumors was significantly higher than that of WT tumors (Figure 4B), suggesting that host-derived CCL21-Ser negatively regulates hematopoietic cell infiltration into the tumor tissues. The CCR7<sup>+</sup> proportion of CD45<sup>+</sup> cells was significantly higher in F10-ccl21 tumors than F10-mock

tumors in WT and *Ccl21a*-KO mice, suggesting that melanoma cell-derived CCL21-Ser promotes CCR7<sup>+</sup> cell infiltration into tumor tissues. The CCR7<sup>+</sup> cell percentage in F10-mock tumors was lower in *Ccl21a*-KO mice than in WT mice, indicating that the CCR7<sup>+</sup> cells are less efficient at infiltrating tumor tissues lacking host- and melanoma cell-derived CCL21-Ser.

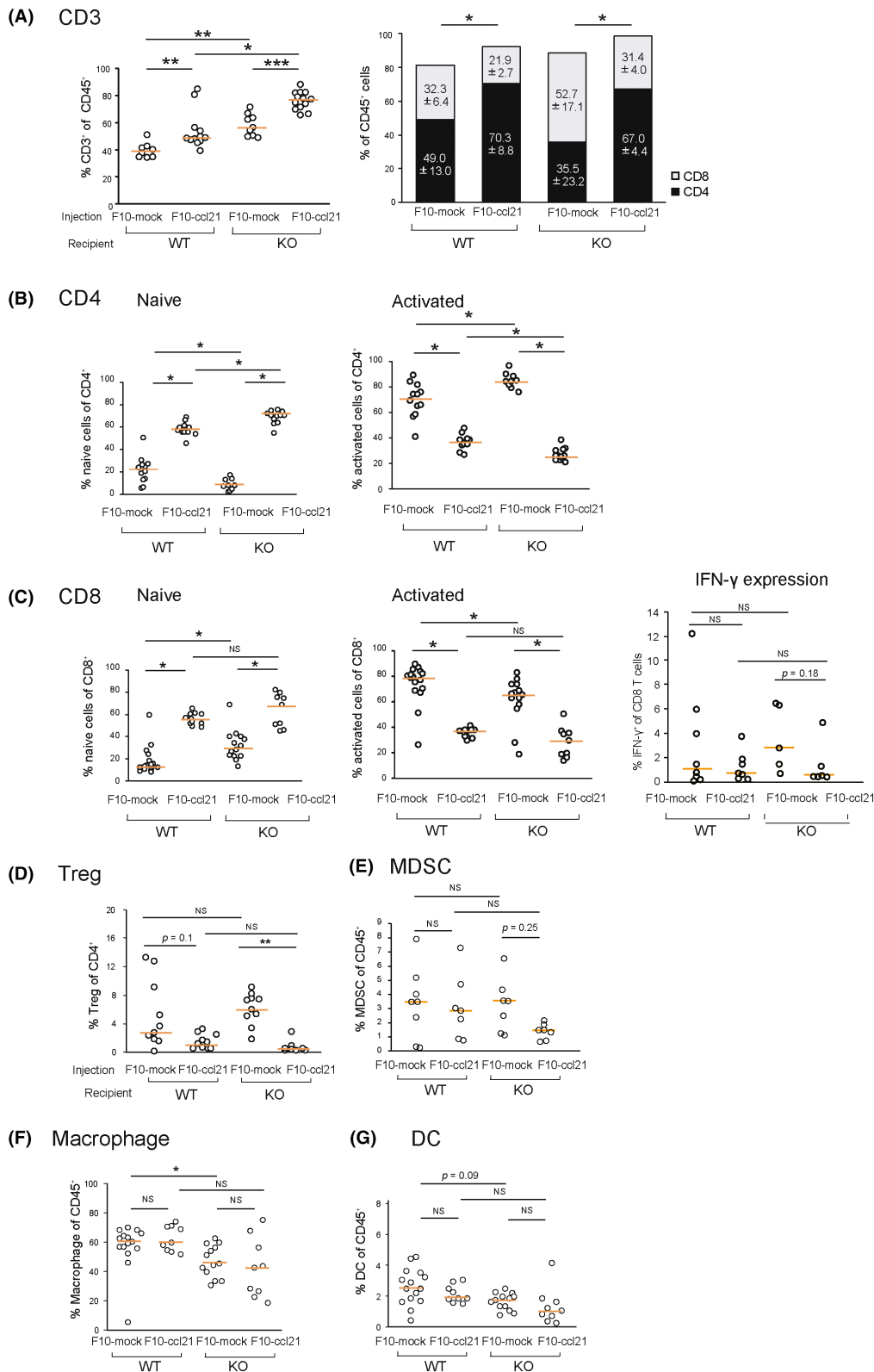


**FIGURE 3** Expression of *Ccl21a* increases naïve T cell frequency and reduces the CD8/CD4 ratio of intratumoral T cells. Intratumoral T cells of F10-mock (WT;  $n = 14$ , KO;  $n = 13$ ) and F10-ccl21 (WT;  $n = 14$ , KO;  $n = 15$ ) tumors were analyzed by flow cytometry. (A) Proportion of CD3<sup>+</sup> T cells and CD8/CD4 ratio, (B, C) naïve (CD44<sup>-</sup> CD62L<sup>+</sup>), activated (CD44<sup>+</sup> CD62L<sup>-</sup>) CD4<sup>+</sup> and CD8<sup>+</sup> cells, IFN- $\gamma$ <sup>+</sup> CD8<sup>+</sup> cells, (D–G) Tregs, myeloid-derived suppressor cells (MDSCs), macrophages, and dendritic cells (DCs) of the CD45<sup>+</sup> hematopoietic cells in F10-mock (WT;  $n = 12$ , KO;  $n = 9$ ) and F10-ccl21 (WT;  $n = 11$ , KO;  $n = 12$ ) tumors. The plot represents individual tumor samples obtained from three to five experimental repeats with one to four mice in each group. The data were analyzed using the Kruskal–Wallis test with the Steel–Dwass post-hoc test. Orange lines show the median. \* $p < 0.05$ , \*\* $p < 0.01$ , \*\*\* $p < 0.001$ . NS, not significant. KO, knockout; WT, wild-type.



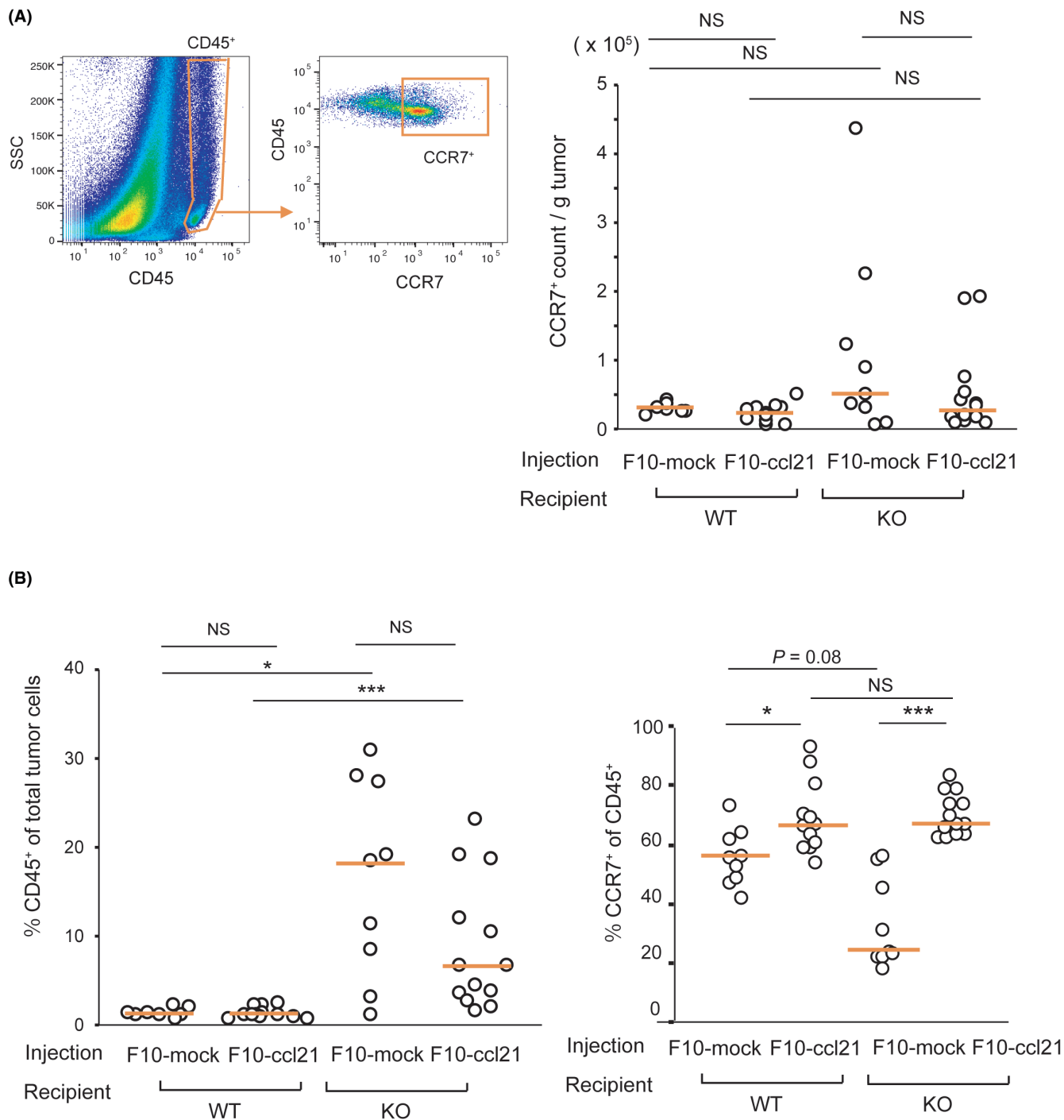


**FIGURE 4** Expression of *Ccl21a* increases the frequency of intratumoral CCR7<sup>+</sup> cells. (A) The intratumoral hematopoietic cells were distinguished by the CD45 expression and side scatter profiles (top), and the number of CCR7<sup>+</sup> cells per tumor weight (bottom) is shown. (B) The percentage of CD45<sup>+</sup> hematopoietic cells and CCR7<sup>+</sup> cells of CD45<sup>+</sup> cells is shown. Tumor cells derived from F10-mock (WT;  $n=8$ , KO;  $n=9$ ) and F10-ccl21 (WT;  $n=12$ , KO;  $n=13$ ) were analyzed. The plot represents individual tumor samples obtained from three to five experimental repeats with two to four mice in each group. The data were analyzed using the Kruskal–Wallis test with the Steel–Dwass post-hoc test. Orange lines show the median. \* $p < 0.05$ , \*\*\* $p < 0.001$ . NS, not significant. KO, knockout; WT, wild-type.

We next characterized tumor-infiltrated CCR7<sup>+</sup> subsets. The FSC/SSC profiles revealed that lymphocytes were remarkably increased in F10-ccl21 tumors in *Ccl21a*-KO mice (Figure 5). Among lymphocytes, CD62L<sup>+</sup> T cells were significantly increased, whereas activated T and B cells were not increased by CCL21-Ser expression.

Although macrophages and DCs were included in the CCR7<sup>+</sup> cells, their proportion was not changed by CCL21-Ser expression. These results suggest that tumor-derived CCL21-Ser expression promotes the accumulation of CCR7<sup>+</sup> subsets, most preferentially CD62L<sup>+</sup> naïve T cells.

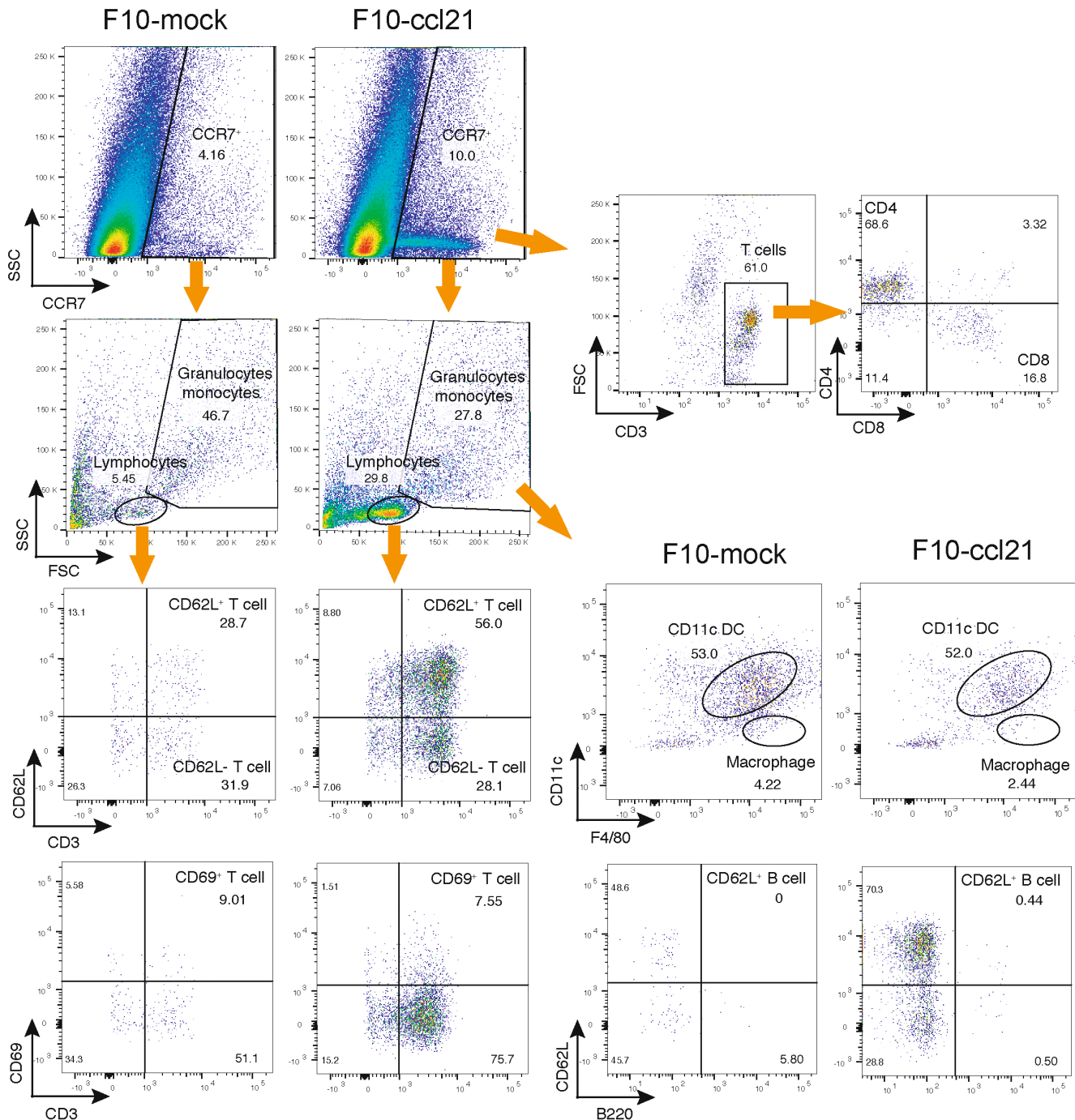


**FIGURE 5** Naïve T cells are most frequently recruited into *Ccl21a*-expressing tumors. The intratumoral CCR7<sup>+</sup>, CD62L<sup>+</sup>, CD3<sup>+</sup>, CD4<sup>+</sup>, CD8<sup>+</sup>, CD69<sup>+</sup>, B220<sup>+</sup>, CD11c<sup>+</sup>, and F4/80<sup>+</sup> cell were analyzed by flow cytometry. Representative data from two independent experiments with F10-mock ( $n=2$ ) and F10-ccl21 ( $n=4$ ) in *Ccl21a*-KO mice are shown.

Under physiological conditions, naïve lymphocytes circulate between the secondary lymphoid tissues and blood. Therefore, we examined whether the preferential migration of naïve T cells into the tumor tissues in CCL21-Ser-expressing tumors affects the number of naïve T cells in tumor-draining LNs (TDLNs). The CD44<sup>lo</sup>CCR7<sup>+</sup> naïve T cell count in TDLNs of CCL21-Ser-expressing tumors was significantly lower than those of F10-mock tumors in WT mice, and a similar trend was also observed in the *Ccl21a*-KO mice (Figure 6A).

These observations support the idea that naïve T cells are preferentially recruited into CCL21-Ser-expressing tumors. Macrophage and DC counts were unchanged by CCL21-Ser expression in tumors, although the macrophage counts in TDLN was increased in *Ccl21a*-KO mice carrying CCL21-Ser expressing tumors (Figure S4).

To assess the possibility of examining lymphocyte migration from blood into tumor tissues, we adoptively transferred GFP<sup>+</sup> T cells into tumor-bearing mice. As shown in Figure 6B, the CD62L<sup>+</sup> T cells

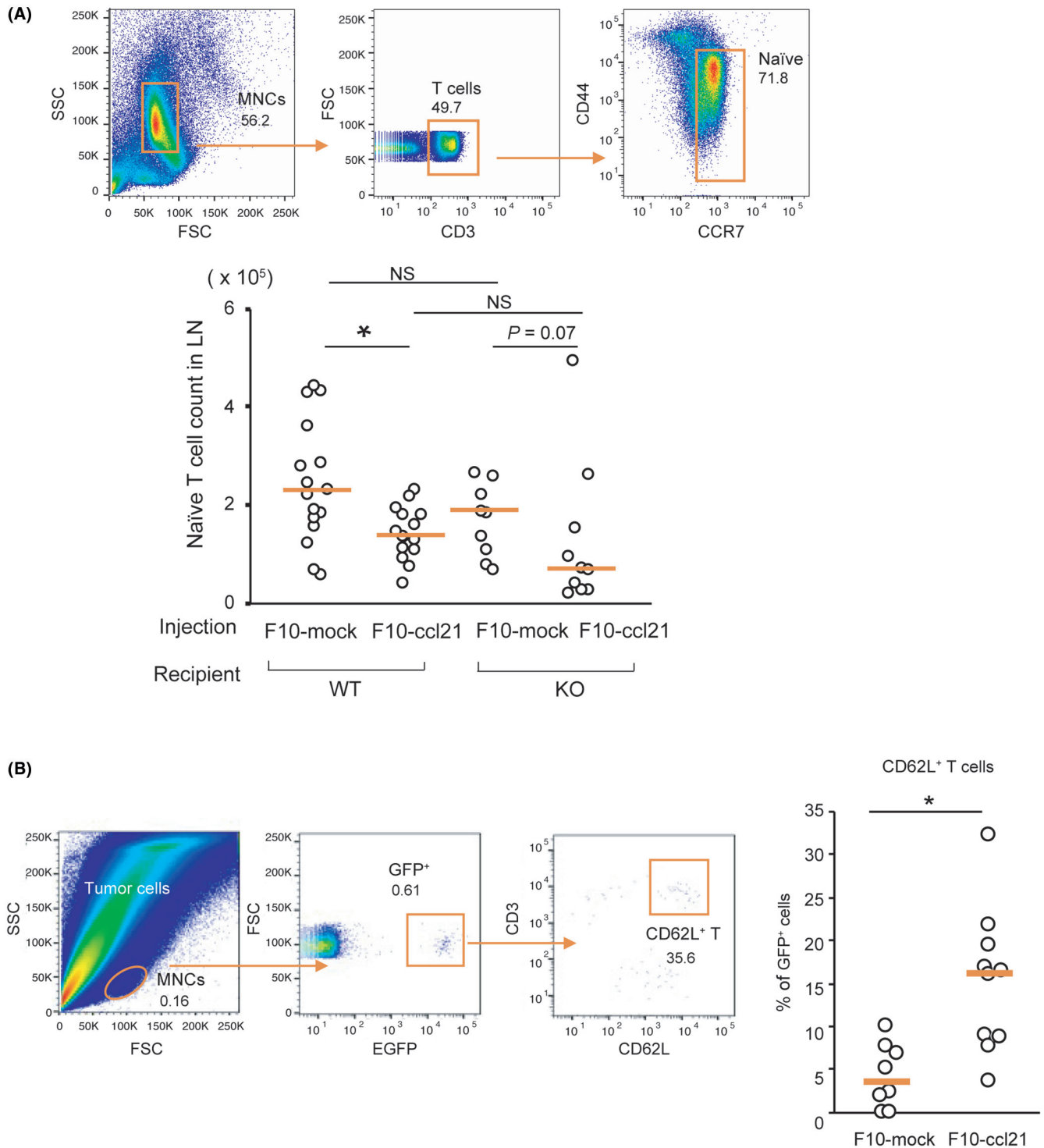


**FIGURE 6** Naive T cells preferentially migrate into *Ccl21a*-expressing tumors. (A) The number of naive T cells in the tumor-draining lymph nodes (TDLNs) of tumor-bearing mice. Mononuclear cells (MNCs) in the TDLNs were distinguished by the FSC/SSC profile, and frequencies of CD44<sup>+</sup> CCR7<sup>+</sup> naive T cells of CD3<sup>+</sup> cells were analyzed. Each plot shows each lymph node (LN) sample of WT or KO mice carrying F10-mock (WT;  $n = 17$ , KO;  $n = 10$ ) and F10-*ccl21a* tumor (WT;  $n = 15$ , KO;  $n = 9$ ). (B) F10-mock and F10-*ccl21a* tumors generated in WT mice were harvested 24 h after intravenous injection of GFP<sup>+</sup> splenocytes. MNCs in tumors derived from F10-mock and F10-*ccl21a* were distinguished by the FSC/SSC profile, and the proportion of CD62L<sup>+</sup> CD3<sup>+</sup> naive T cells of GFP<sup>+</sup> cells that have migrated into the tumor-carrying WT mice are shown (F10-mock:  $n = 8$ , F10-*ccl21a*:  $n = 10$ ). The data were analyzed by the Steel–Dwass test or the Mann–Whitney *U*-test. Orange lines show the median. \* $p < 0.05$ , NS, not significant. KO, knockout; WT, wild-type.

migrated more efficiently into F10-ccl21-derived tumors than into F10-mock tumors 24 h after injection. In contrast, T cells migrated to the spleen and LNs at comparable levels between F10-ccl21-bearing and F10-mock-bearing mice, suggesting that melanoma cell-derived CCL21-Ser does not affect naïve lymphocyte migration into the secondary lymphoid tissues (Figure S5).

We next assessed the activation status of CD4 and CD8 T cells in TDLNs. Although the expression of activation marker molecule CD69 was unchanged, IFN- $\gamma$  expression on CD4 and CD8 T cells was elevated in F10-ccl21-bearing *Ccl21a*-KO mice compared with other groups (Figure S6). These results suggest that the immune response in TDLNs is efficiently induced in the absence of CCL21-Ser expression.

To explore whether *CCL21* expression is correlated to the immune cell profiles in human melanoma, we extracted the gene expression profile of human melanoma from The Cancer Genome Atlas (TCGA) database and examined *CCL21* expression. TCGA profiles indicate that *CCL21* expression is at various levels (Figure S7a). The CIBERSORT deconvolution algorithm revealed that naïve CD4 T-cell frequency tends to increase, while activated CD4 frequency decreases significantly with increasing *CCL21* expression. These results are consistent with what we observed in mouse B16-F10 melanomas. In contrast, Tregs are clearly increased in *CCL21*-expressing human melanomas, unlike what we observed in mouse melanomas (Figure S7b). We also found that the frequency of lymphocyte infiltration is positively correlated with their CCR7 expression levels (Figure S7c), suggesting that CCR7-expressing lymphocytes are preferentially recruited to melanoma tissues in response to CCL21 expression.

## 4 | DISCUSSION

Herein, we assessed the function of tumor-derived CCL21-Ser using *CCL21a*-deficient mice, where the influence of host-derived CCL21-Ser was completely eliminated. We demonstrated that reduced tumor growth in *CCL21a*-KO mice was restored by CCL21-Ser expression from melanomas. This observation suggests that melanoma-derived CCL21-Ser contributes to tumor growth, supporting the idea proposed by Shields et al.; they demonstrated that the CCL21-Ser expression in B16-F10 enhances tumor growth in WT mice.<sup>16</sup> In our study, melanoma growth was decreased in *Ccl21a*-KO mice compared with that in WT mice, indicating that host-derived CCL21-Ser contributes to tumor growth. Since the parental B16-F10 cells express neither *Ccl21a* nor *Ccr7* at levels detectable by RT-PCR analysis in our previous study,<sup>18</sup> it is unlikely that CCL21-Ser acts through CCR7 expression in B16-F10 cells. These data suggest that CCR7-positive cells in the recipient mice regulate antitumor immunity and melanoma growth.

Our study demonstrated that a prominent increase in the frequency of tumor-infiltrated CD62L<sup>+</sup> T cells corresponds with melanoma growth, suggesting that the accumulation of naïve T cells in tumors is primarily responsible for tumor growth. The estimated

CCL21-Ser concentration of F10-ccl21 culture supernatant was approximately 600 ng/mL, and a previously reported CCL21 concentration that induces in vitro mouse T cell chemotaxis most efficiently is 500 ng/mL.<sup>29</sup> Given that the CCL21 concentrations in LNs and spleens have been estimated to be 11,000–12,000 ng/mL,<sup>30</sup> 600 ng/mL CCL21 is estimated to be a sufficient concentration to attract T cells to tumor tissues. Thus, as a mechanism by which CCR7<sup>+</sup> cells accumulate in CCL21-expressing tumors, we speculate that tumor-derived CCL21 acts on CCR7-positive cells and recruits them to the tumor tissues.

We demonstrated that the number of naïve T cells in the TDLN of CCL21-Ser-expressing tumors was reduced compared to that of tumors not expressing CCL21-Ser. These results suggest that tumor-derived CCL21-Ser affects the number of lymphocytes in the TDLN. The decreased lymphocyte counts in the TDLN of CCL21-Ser-expressing tumors correlated with decreased IFN- $\gamma$  expression in the TDLN and tumors, indicating a decreased immune response in CCL21-Ser-expressing tumors. These data are consistent with a previous report that a decrease in naïve lymphocytes in LNs causes a reduced immune response.<sup>31</sup> The adoptive transfer experiments with GFP<sup>+</sup> spleen cells did not provide evidence of reduced cell migration to LNs, suggesting that naïve T lymphocyte count in F10-ccl21 tumor-draining LNs was affected over the long term. Mechanisms other than decreased lymphocyte migration should also be considered: for example, decreased retention of lymphocytes in LNs or enhanced migration from draining lymph vessels. The mechanism of the decrease in lymphocyte count needs to be evaluated in future studies.

Regarding a possible mechanism by which CCL21-Ser expression promotes tumor growth, earlier studies have shown that tumor-derived lactate promotes apoptosis of naïve T cells, resulting in increased tumor immune resistance and tumor growth.<sup>32</sup> However, this possibility seems unlikely in our experimental setting, as our preliminary data showed no trend toward increased apoptosis of naïve T cells in tumors expressing CCL21-Ser. The influence of naïve T cells on the tumor microenvironment is an essential topic for future studies.

There has been increasing evidence suggesting that Tregs and MDSCs are characterized by their ability to suppress antitumor immune response mediated by various immune cell populations, and they are closely associated with poor clinical outcomes in cancer.<sup>25,33</sup> A previous report proposed that both Tregs and Gr-1<sup>+</sup>CD11b<sup>+</sup> MDSCs provide tolerogenic tumor microenvironment by CCL21-Ser expression in B16-F10 tumors.<sup>16</sup> Consistent with the earlier study, MDSCs infiltration was increased by CCL21-Ser expression. MDSCs express CCR7;<sup>34</sup> therefore, MDSCs potentially migrate in response to CCL21-expressing tumors through CCR7 and regulate melanoma growth. In contrast to MDSCs, Treg infiltration was reduced by CCL21-Ser expression in our study, suggesting that Tregs are unlikely to be responsible for melanoma growth. The discrepancy in the change of Treg infiltration by CCL21-Ser expression may be explained by the level of tertiary lymphoid structures (TLS) formation, which we could not detect in F10-ccl21a-derived tumors.

The earlier study suggested that CCL21 expression causes the formation of stromal network structures by infiltration of CCR7<sup>+</sup> lymphoid tissue-induced cells and supports the recruitment of Tregs to these structures.<sup>16</sup> Although Tregs are present in TLS and non-TLS areas, and both Tregs show similar gene expression profiles, TLS Tregs overexpress CCR7 compared to non-TLS Tregs.<sup>27</sup> We were not able to detect TLS in B16-F10-derived tumors in this study, and Tregs expressing high levels of CCR7 may not have increased due to insufficient recruitment to the tumor in the absence of lymphoid tissue-like structures expressing CCL21-Ser.

The study of human melanoma partially supports the contribution of tumor-derived CCL21 expression to immune cell composition of mouse melanoma, with a trend toward increased naïve CD4<sup>+</sup> T cells and decreased activated CD4<sup>+</sup> cells. In contrast, human melanomas show an increased frequency of Tregs by CCL21 expression, which is inconsistent with the results in the mouse model. The discrepancy in Treg infiltration may be due to differences in the stage of the human samples obtained, the period of treatment, and the presence or absence of lymphoid tissue-like structures in the tissues. In addition, the CIBERSORT algorithm is based on the expression profile of immune cells in non-tumor tissue. However, more than 95% of Tregs in mouse melanomas are CD45RA-negative memory types. Therefore, the analysis may not accurately reflect the frequency of these cells.

We currently have no evidence suggesting the involvement of macrophages and DCs in tumor growth. Although the number of macrophages and DCs in the tumor and their frequency relative to leukocytes tended to be reduced by the expression of CCL21-Ser from melanoma cells, there was no statistical difference. In B16 melanoma tissues, CCL21 expression correlates with TGFβ1 expression.<sup>16</sup> TGFβ1 shifts the macrophage population from tumor-suppressive M1 macrophages to tumor-promotive M2 macrophages.<sup>35,36</sup> Although the ratio of M1 to M2 was not evaluated in this study, the shift from M1 to M2 may be responsible for tumor growth. It also remains unclear whether CCL21-Ser expression in tumors affects the efficiency of CCR7-dependent DC migration from tumor lesion to TDLN. It is possible that the inadequate CCL21-Ser concentration gradient between the regional LNs and CCL21-Ser expression in tumor tissues hampers the CCR7-dependent migration of activated DCs into the regional LNs, resulting in a reduced antitumor immune response. In addition, the influence of CCL21-Leu expressed in intra-tumoral lymphatic vessels should also be considered for DC migration. In mice lacking CCL19 and CCL21-Ser, DCs migrated into peripheral lymphatic vessels but showed impaired trafficking into and within the LN stroma despite the expression of CCL21-Leu, suggesting that CCL21-Ser plays critical roles in dendritic cell localization, whereas CCL21-Leu is important for DC entry into peripheral lymphatics.<sup>8</sup> The contribution of CCL21-Leu to immune reaction in TDLNs needs to be analyzed in the future.

In summary, we demonstrated that in addition to the host-derived and melanoma cell-derived CCL21-Ser supports tumor growth in vivo. Our study suggests that immunosuppression by Tregs is not primarily involved and that naïve T cells and possibly

MDSCs contribute to melanoma growth. Future analyses focusing on the effect of increased naïve T cell and MDSC infiltration into tumor tissues are expected to clarify the mechanism of CCL21-Ser-dependent antitumor immunity.

#### AUTHOR CONTRIBUTIONS

H.H. designed the experiments and wrote the manuscript. M.M., Y.K., R.F., K.K., K.F., R.N., R.H., and I.K. performed most of the experiments and analyses. I.K. and I.O. critically reviewed and revised the manuscript. All authors reviewed and approved the final manuscript.

#### ACKNOWLEDGMENTS

We thank Drs Yousuke Takahama (National Institutes of Health), Tomoya Katakai (Niigata University), Michio Tomura (Osaka Ohtani University), and Eiji Umemoto (University of Shizuoka) for helpful suggestions; the Division of Joint Research Center, Kindai University for granting access to a flow cytometer and an IVIS Imaging System; and Enago ([www.enago.jp](http://www.enago.jp)) for its English language review.

#### FUNDING INFORMATION

This work is supported by the Ministry of Education, Culture, Sports, Science and Technology, Japan (Grant-in-Aid for Scientific Research, 22K06823 to H.H.)

#### CONFLICT OF INTEREST STATEMENT

The authors have no conflict of interest.

#### ETHICS STATEMENT

Approval of the research protocol: All experiments were conducted in accordance with the approved guidelines from Kindai University. Informed Consent: N/A.

Registry and the Registration No. of the study/trial: N/A.

Animal Studies: The experimental protocols for the use of laboratory animals were approved by the Ethics Review Committee of Kindai University (KASE-2021-001).

#### ORCID

Haruko Hayasaka  <https://orcid.org/0000-0003-1694-9248>

#### REFERENCES

- Gunn MD, Tangemann K, Tam C, Cyster JG, Rosen SD, Williams LT. A chemokine expressed in lymphoid high endothelial venules promotes the adhesion and chemotaxis of naïve T lymphocytes. *Proc Natl Acad Sci U S A*. 1998;95:258-263.
- Willmann K, Legler DF, Loetscher M, et al. The chemokine SLC is expressed in T cell areas of lymph nodes and mucosal lymphoid tissues and attracts activated T cells via CCR7. *Eur J Immunol*. 1998;28:2025-2034.
- Kozai M, Kubo Y, Katakai T, et al. Essential role of CCL21 in establishment of central self-tolerance in T cells. *J Exp Med*. 2017;214:1925-1935.
- Nakano H, Gunn MD. Gene duplications at the chemokine locus on mouse chromosome 4: multiple strain-specific haplotypes and the deletion of secondary lymphoid-organ chemokine and EBI-1 ligand chemokine genes in the plt mutation. *J Immunol*. 2001;166:361-369.

5. Yoshida R, Nagira M, Kitaura M, Imagawa N, Imai T, Yoshie O. Secondary lymphoid-tissue chemokine is a functional ligand for the CC chemokine receptor CCR7. *J Biol Chem*. 1998;273:7118-7122.
6. Chen SC, Vassileva G, Kinsley D, et al. Ectopic expression of the murine chemokines CCL21a and CCL21b induces the formation of lymph node-like structures in pancreas, but not skin, of transgenic mice. *J Immunol*. 2002;168:1001-1008.
7. Forster R, Schubel A, Breitfeld D, et al. CCR7 coordinates the primary immune response by establishing functional microenvironments in secondary lymphoid organs. *Cell*. 1999;99:23-33.
8. Gunn MD, Kyuwa S, Tam C, et al. Mice lacking expression of secondary lymphoid organ chemokine have defects in lymphocyte homing and dendritic cell localization. *J Exp Med*. 1999;189:451-460.
9. Kurobe H, Liu C, Ueno T, et al. CCR7-dependent cortex-to-medulla migration of positively selected thymocytes is essential for establishing central tolerance. *Immunity*. 2006;24:165-177.
10. James KD, Legler DF, Purvanov V, et al. Medullary stromal cells synergize their production and capture of CCL21 for T-cell emigration from neonatal mouse thymus. *Blood Adv*. 2021;5:99-112.
11. Mashino K, Sadanaga N, Yamaguchi H, et al. Expression of chemokine receptor CCR7 is associated with lymph node metastasis of gastric carcinoma. *Cancer Res*. 2002;62:2937-2941.
12. Ding YZ, Shimada Y, Maeda M, et al. Association of CC chemokine receptor 7 with lymph node metastasis of esophageal squamous cell carcinoma. *Clin Cancer Res*. 2003;9:3406-3412.
13. Takanami I. Overexpression of CCR7 mRNA in nonsmall cell lung cancer: correlation with lymph node metastasis. *Int J Cancer*. 2003;105:186-189.
14. Wiley HE, Gonzalez EB, Maki W, Wu MT, Hwang ST. Expression of CC chemokine receptor-7 and regional lymph node metastasis of B16 murine melanoma. *J Natl Cancer Inst*. 2001;93:1638-1643.
15. Cunningham HD, Shannon LA, Calloway PA, et al. Expression of the C-C chemokine receptor 7 mediates metastasis of breast cancer to the lymph nodes in mice. *Transl Oncol*. 2010;3:354-361.
16. Shields JD, Kourtis IC, Tomei AA, Roberts JM, Swartz MA. Induction of lymphoidlike stroma and immune escape by tumors that express the chemokine CCL21. *Science*. 2010;328:749-752.
17. Peske JD, Thompson ED, Gemta L, Baylis RA, Fu YX, Engelhard VH. Effector lymphocyte-induced lymph node-like vasculature enables naïve T-cell entry into tumours and enhanced anti-tumour immunity. *Nat Commun*. 2015;6:15.
18. Fujie R, Yamada Y, Fujiwara K, et al. An endogenous CCL21-Ser deficiency reduces melanoma growth by an enhanced antitumor immunity. 2022. doi:10.21203/rs.3.rs-1500142/v1
19. Newman AM, Liu CL, Green MR, et al. Robust enumeration of cell subsets from tissue expression profiles. *Nat Methods*. 2015;12:453-457.
20. Chen B, Khodadoust MS, Liu CL, Newman AM, Alizadeh AA. Profiling tumor infiltrating immune cells with CIBERSORT. *Methods Mol Biol*. 2018;1711:243-259.
21. van Elsas A, Hurwitz AA, Allison JP. Combination immunotherapy of B16 melanoma using anti-cytotoxic T lymphocyte-associated antigen 4 (CTLA-4) and granulocyte/macrophage colony-stimulating factor (GM-CSF)-producing vaccines induces rejection of subcutaneous and metastatic tumors accompanied by autoimmune depigmentation. *J Exp Med*. 1999;190:355-366.
22. Shimizu J, Yamazaki S, Sakaguchi S. Induction of tumor immunity by removing CD25<sup>+</sup>CD4<sup>+</sup> T cells: a common basis between tumor immunity and autoimmunity. *J Immunol*. 1999;163:5211-5218.
23. Turk MJ, Guevara-Patino JA, Rizzuto GA, Engelhorn ME, Houghton AN. Concomitant tumor immunity to a poorly immunogenic melanoma is prevented by regulatory T cells. *J Exp Med*. 2004;200:771-782.
24. Li K, Shi H, Zhang B, et al. Myeloid-derived suppressor cells as immunosuppressive regulators and therapeutic targets in cancer. *Signal Transduct Target Ther*. 2021;6:362.
25. Veglia F, Gabrilovich DI. Dendritic cells in cancer: the role revisited. *Curr Opin Immunol*. 2017;45:43-51.
26. DeNardo DG, Ruffell B. Macrophages as regulators of tumour immunity and immunotherapy. *Nat Rev Immunol*. 2019;19:369-382.
27. Devi-Marulkar P, Fastenackels S, Karapentantz P, et al. Regulatory T cells infiltrate the tumor-induced tertiary lymphoid structures and are associated with poor clinical outcome in NSCLC. *Commun Biol*. 2022;5:1416.
28. Forster R, Davalos-Misslitz AC, Rot A. CCR7 and its ligands: balancing immunity and tolerance. *Nat Rev Immunol*. 2008;8:362-371.
29. Bai Z, Hayasaka H, Kobayashi M, et al. CXC chemokine ligand 12 promotes CCR7-dependent naïve T cell trafficking to lymph nodes and Peyer's patches. *J Immunol*. 2009;182:1287-1295.
30. Luther SA, Bidgol A, Hargreaves DC, et al. Differing activities of homeostatic chemokines CCL19, CCL21, and CXCL12 in lymphocyte and dendritic cell recruitment and lymphoid neogenesis. *J Immunol*. 2002;169:424-433.
31. Denton AE, Roberts EW, Linterman MA, Fearon DT. Fibroblastic reticular cells of the lymph node are required for retention of resting but not activated CD8<sup>+</sup> T cells. *Proc Natl Acad Sci U S A*. 2014;111:12139-12144.
32. Xia H, Wang W, Crespo J, et al. Suppression of FIP200 and autophagy by tumor-derived lactate promotes naïve T cell apoptosis and affects tumor immunity. *Sci Immunol*. 2017;2:eaan4631.
33. Shevryev D, Tereshchenko V. Treg heterogeneity, function, and homeostasis. *Front Immunol*. 2019;10:3100.
34. Suk Lee Y, Davila E, Zhang T, et al. Myeloid-derived suppressor cells are bound and inhibited by anti-thymocyte globulin. *Innate Immun*. 2019;25:46-59.
35. Bierie B, Moses HL. Tumour microenvironment: TGFbeta: the molecular Jekyll and Hyde of cancer. *Nat Rev Cancer*. 2006;6:506-520.
36. Sica A, Larghi P, Mancino A, et al. Macrophage polarization in tumour progression. *Semin Cancer Biol*. 2008;18:349-355.

## SUPPORTING INFORMATION

Additional supporting information can be found online in the Supporting Information section at the end of this article.

**How to cite this article:** Miyamoto M, Kawato Y, Fujie R, et al. CCL21-Ser expression in melanoma cells recruits CCR7<sup>+</sup> naïve T cells to tumor tissues and promotes tumor growth. *Cancer Sci*. 2023;114:3509-3522. doi:[10.1111/cas.15902](https://doi.org/10.1111/cas.15902)